REPORT DOCUMENTATION PAGE

Form Approved
OMB No. 0704-0188

1. REPORT DATE *(DD-MM-YYYY)*	**2. REPORT TYPE**	**3. DATES COVERED** *(From - To)*
June 2013	Technical Paper	June 2013-July 2013

4. TITLE AND SUBTITLE
Combustion Instability Mechanisms in a Pressure-coupled Gas-gas Coaxial Rocket Injector

5a. CONTRACT NUMBER
In-House

5b. GRANT NUMBER

5c. PROGRAM ELEMENT NUMBER

6. AUTHOR(S)
Harvazinski, M. , Huang, C., Sankaran, V., Feldman, T., Anderson, W., Merkle, C., and Talley, D.

5d. PROJECT NUMBER

5e. TASK NUMBER

5f. WORK UNIT NUMBER
Q0A1

7. PERFORMING ORGANIZATION NAME(S) AND ADDRESS(ES)

Air Force Research Laboratory (AFMC)
AFRL/RQRC
10 E. Saturn Blvd.
Edwards AFB CA 93524-7680

8. PERFORMING ORGANIZATION REPORT NO.

9. SPONSORING / MONITORING AGENCY NAME(S) AND ADDRESS(ES)
Air Force Research Laboratory (AFMC)
AFRL/RQR
5 Pollux Drive
Edwards AFB CA 93524-7048

10. SPONSOR/MONITOR'S ACRONYM(S)

11. SPONSOR/MONITOR'S REPORT NUMBER(S)
AFRL-RQ-ED-TP-2013-157

12. DISTRIBUTION / AVAILABILITY STATEMENT
Distribution A: Approved for Public Release; Distribution Unlimited. PA#13362

13. SUPPLEMENTARY NOTES
Conference paper for the 49th AIAA/ASME/SAE/ASEE Joint Propulsion Conference, San Jose, CA, 15-17 July 2013.

14. ABSTRACT
An investigation of the instability mechanism present in a laboratory rocket combustor is performed using computational fluid dynamics (CFD) simulations. Three cases are considered which show different levels of instability experimentally. Computations reveal three main aspects to the instability mechanism, the timing of the pressure pulses, increased mixing due to the baroclinic torque, and the presence of unsteady tribrachial flame. The stable configuration shows that fuel is able to flow into the combustor continuously allowing continuous heat release. The unstable configuration shows that a disruption in the fuel flow into the combustor allows the heat release to move downstream and new fuel to accumulate in the combustor without immediately burning. Once the large amounts of fuel in the combustor burn there is rapid rise in pressure which coincides with the timing of the acoustic wave in the combustor. The two unstable cases show different levels of instability and dfferent reignition mechanism.

15. SUBJECT TERMS

16. SECURITY CLASSIFICATION OF:			**17. LIMITATION OF ABSTRACT**	**18. NUMBER OF PAGES**	**19a. NAME OF RESPONSIBLE PERSON**
					Doug Talley
a. REPORT	**b. ABSTRACT**	**c. THIS PAGE**	SAR	22	**19b. TELEPHONE NO** *(include area code)*
Unclassified	**Unclassified**	**Unclassified**			661-525-6174

Standard Form 298 (Rev. 8-98)
Prescribed by ANSI Std. 239.18

Combustion Instability Mechanisms in a Pressure-coupled Gas-gas Coaxial Rocket Injector

Matthew E. Harvazinski[*]
Air Force Research Laboratory, Edwards AFB, CA, 93524
Cheng Huang[†]
Purdue University, West Lafayette, IN, 47907
Venkateswaran Sankaran[‡]
Air Force Research Laboratory, Edwards AFB, CA, 93524
Thomas W. Feldman[§] William E. Anderson[¶] Charles L. Merkle[‖]
Purdue University, West Lafayette, IN, 47907
and
Douglas G. Talley[**]
Air Force Research Laboratory, Edwards AFB, CA, 93524

An investigation of the instability mechanism present in a laboratory rocket combustor is performed using computational fluid dynamics (CFD) simulations. Three cases are considered which show different levels of instability experimentally. Computations reveal three main aspects to the instability mechanism, the timing of the pressure pulses, increased mixing due to the baroclinic torque, and the presence of unsteady tribrachial flame. The stable configuration shows that fuel is able to flow into the combustor continuously allowing continuous heat release. The unstable configuration shows that a disruption in the fuel flow into the combustor allows the heat release to move downstream and new fuel to accumulate in the combustor without immediately burning. Once the large amounts of fuel in the combustor burn there is rapid rise in pressure which coincides with the timing of the acoustic wave in the combustor. The two unstable cases show different levels of instability and different reignition mechanism.

Nomenclature

p	Pressure
p'	Pressure Fluctuation
$\dot{q}'$	Heat Release Fluctuation
$\mathscr{R}$	Rayleigh Index
t	Time
T	Integration Period
$\mathbf{u}$	Velocity Vector
$\mathbf{x}$	Spatial Coordinate
Z	Mixture Fraction
ρ	Density

[*]Scientist, AIAA Member.
[†]Graduate Research Assistant, AIAA Student Member.
[‡]Senior Scientist, AIAA Member.
[§]Graduate Research Assistant, AIAA Student Member.
[¶]Professor, AIAA Associate Fellow.
[‖]Professor Emeritus, AIAA Member.
[**]Research Physical Scientist, AIAA Associate Fellow.

$\boldsymbol{\tau}$ Stress Tensor
$\boldsymbol{\omega}$ Vorticity

I. Introduction

Combustion instabilities are encountered in a variety of combustion devices including liquid and solid rocket engines, gas turbines, and ramjets. Instabilities are the result of an interaction between the acoustics, geometry, and combustion. Varying levels of instabilities can arise and are almost always unwanted because of the increased vibrations, increased local heat transfer, flashback, and the uncontrolled impulse that can result. The uncontrolled impulse can cause damage to the injector or in the most extreme case cause a catastrophic failure of the engine. Rockets are particularly problematic because they are acoustically compact. The acoustic waves generated when combustion takes place can reflect off of boundaries. When the acoustic waves travel back to the region of combustion they can influence the local fluid mechanics and the combustion taking place there.[1–3]

When combustion takes place it is possible for a feedback path to become established where increasing pressure leads to increasing heat release which in turn leads to increasing pressure. Despite the existence of this relatively simple feedback path, there is no simple predictive model that can accurately determine when a particular combination of geometry and operating conditions will result in an instability. A large amount of work has been done using linear analysis where a wave equation is augmented with a heat release source term. The limitation is that the heat release is frequently a response function that must be derived from experimental or detailed computational data. Linear methods are also limited in that only the initial growth is described; limit cycle behavior cannot be captured. Linear methods also presume that the amplitude of the heat releases response is linearly proportional to the perturbation and that the response frequency is the same as the perturbation frequency, whereas, in fact, coupling mechanisms are much more complex.[4–6] Non-linear analysis can be done with non-linear acoustics, non-linear combustion, or both. A paper by Culick noted that without combustion there would be no instability yet most of the non-linear analysis has focused on the acoustics.[7] The difficulty is that an accurate description of the energy gains and losses is required to develop a truly predictive model. Large eddy simulations (LES) of reacting flow are well suited for this task assuming that models that can accurately represent the physics are used. The advantage of LES is the coupled nature of the governing equations that determine the solution to all parameters of interest at every spatial location and instance in time thus providing spatially and temporally resolved heat release and acoustics.

This work focuses on the simulation of the continuously variable resonance chamber or CVRC experiment conducted at Purdue University. The CVRC experiment has generated a large amount of both stable and unstable data. The CVRC experiment is the third iteration of an unstable laboratory rocket combustor experiment at Purdue. Work first done by Miller used a radial inlet for the oxidizer and liquid JP-8 for the fuel; the length of the combustor was variable and could be changed by adding or removing sections, different lengths gave different amplitudes of longitudinal instability as well as different dominant modes.[8,9]

Following Miller's work was a second iteration by Sisco, who varied the backstep height and discretely changed the length of the oxidizer inlet to generate different levels of instability. Using a smaller backstep larger amplitude pressure oscillations were observed. It was speculated that the vortex shedding at the backstep, which would be different in each case, was responsible for the differences in the instability magnitude. These experiments again used liquid JP-8.[10] The trend in backstep height was successfully modeled by Smith et al. Simulations showed that vortex impingement occurred closer to the backstep for the small step height; this impingement timing was closely aligned with the unstable acoustic mode. For the larger step height, the impingement occurred further downstream and the vortex partially decayed before impingement, the timing of this event was not well correlated with the acoustic mode.[11]

For the third iteration an effort was made to design the experimental rig with CFD validation in mind. Yu replaced the radial oxidizer injector with series of choked slots aligned in the axial direction, this allowed for both axisymmetric and three-dimensional modeling. The fuel was also switched to gaseous methane eliminating the uncertainty associated with atomization models. Perhaps the most interesting change was the ability to vary the oxidizer post as the experiment progressed. The level of instability observed is directly related to the length of the oxidizer post.[12,13] The experiment shows both stable and unstable combustion regimes. Smith et al. completed a companion simulation of the CVRC in two-dimensions showing that some general trends could be captured in two-dimensions but the harmonic nature of the higher modes was not

realized. Higher modes tended to be broad and not well defined unlike the experimental results which have distinct peaks. Simulations also predicted unstable behavior for all oxidizer post lengths while experiments showed stable combustion for the extreme short and long lengths.[14,15]

Continued simulations conducted by Harvazinski et al. for the unstable configurations showed three-dimensional simulations were able to produce larger amplitude pressure oscillations compared to the axisymmetric simulations but still failed to achieve the same sustained level of pressure fluctuations that were observed in the experiment. Three-dimensional simulations however were able to capture the higher order harmonics showing strong, well defined peaks similar to the experiment.[16,17]

Additional experiments by Feldman added optical access to the CVRC in an effort to obtain a qualitative understanding of the combustion process. Optical imagery of the $CH^{\star}$ radical showed clearly that the spatial distribution of unsteady heat released changed significantly with pressure oscillation amplitude.[18] Feldman et al. provided a detailed comparison of the unstable experiment and a three-dimensional simulation. Many features were well captured by the simulation including the steepened wave fronts, rate of pressure rise, and mode shape. The simulation predicted overall lower levels of instability.[19]

Axisymmetric simulations by Smith found the effect of the combustor wall temperature to be minimal.[14] Independent work by Garby et al. showed that imposing a heat flux boundary on the wall of the combustor damped the instability while an adiabatic wall boundary was unstable.[20] Garby et al. also performed a study looking at the predictive capability of two-dimensional simulations and found similar results to Harvazinski et al., namely that two-dimensional simulations were predictive of some phenomena but lacked the ability capture the amplitude of the instability. The existence of a triple flame structure in the combustor was also suggested as a key element in the instability mechanism.[21] Guézennec et al. provided results of an unstable 4.75 in configuration showing the movement of a triple point occurred at the same frequency as the the first longitudinal mode.[22] To date no simulations of stable operating conditions have been published in the literature.

While a substantial amount of work has been done, the fundamental instability mechanisms present in the CVRC are not well understood. This paper aims to address these underlying mechanisms by using parametric hybrid-RANS/LES simulations. In the current article, we utilize existing and new computational results to systematically analyze the complex interaction between the pressure waves and combustion phenomena. Specifically, multiple cases, which show different levels of instability, are interrogated to help identity the dominant behaviors present.

II. Comparison of Computations and Experiments

A. Experimental Overview

The CVRC experiment has been well documented by Yu et al.,[13] this section serves to briefly introduce the experiment and overview some relevant results which will help to anchor the computational results in the subsequent section. The experiment uses gaseous methane for the fuel and decomposed hydrogen peroxide for the oxidizer, a summary of the operating conditions is shown in Table 1. These operating conditions are also used for the simulations. A diagram of the experiment is shown in figure 1. The oxidizer, initially 90% hydrogen peroxide, is fed into the gas generator where it is catalyzed, the oxidizer then enters the manifold as decomposed hydrogen peroxide (conditions shown in table 1). The oxidizer flows through the injector, which is made up of four concentric choked slots. The choked condition in the injector isolates the manifold from the oxidizer post and combustor. The length of the oxidizer post is variable; by translating the injector the oxidizer post can vary from 3.5 in (8.89 cm) to 7.5 in (19.05 cm). Henceforth we will refer to the oxidizer post length in inches. The fuel, gaseous methane, is injected through an annular slot just upstream of the backstep. The combustor is 15 in (38.1 cm) long and a choked converging diverging nozzle is affixed to the end of the combustor.

Table 1: Operating conditions.

Parameter	Value
Fuel Mass Flow Rate, kg/s	0.027
Fuel Temperature, K	300
Oxidizer Mass Flow Rate, kg/s	0.320
Oxidizer Temperature, K	1030
Oxidizer Percent H_2O	57.6
Oxidizer Percent O_2	42.4
Equivalence Ratio	0.8

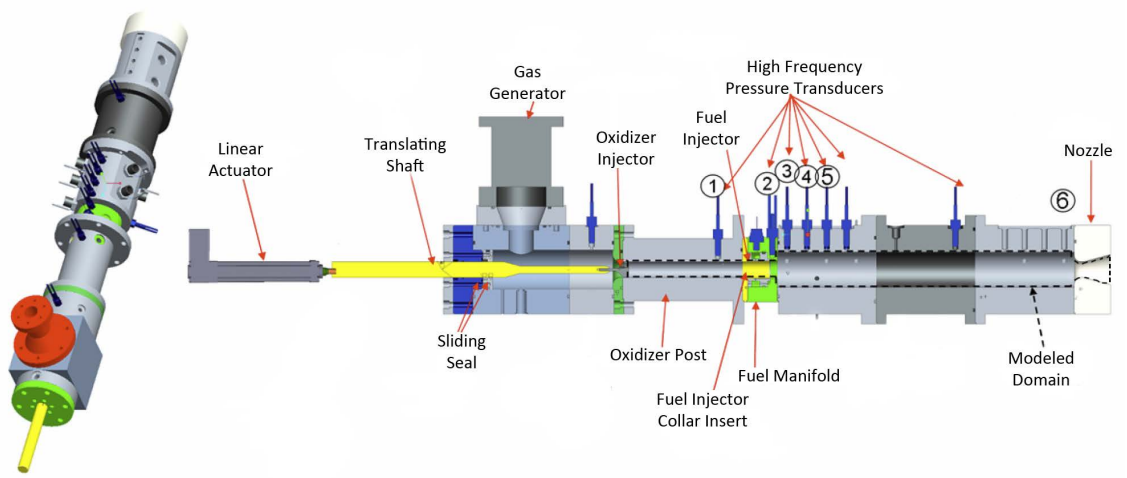

Figure 1: Diagram of the CVRC experiment.

B. Computational Approach

Simulations used the General Equation and Mesh Solver or GEMS developed at Purdue University. GEMS solves the coupled Navier-Stokes equations along with a single energy equation and coupled species equations.[23–28] The numerical scheme is second order accurate in both time and space and uses an implicit formulation which allows for the use of high-aspect ratio grids near the wall. A dual-time formulation is used to eliminate approximate factorization errors. Turbulence is modeled using a hybrid RANS/LES formulation[29,30] where the near wall is modeled using a two-equation k-ω model.[31,32] Combustion is accounted for using a single step global reaction.[33] Global reactions allow for the coupling between pressure and heat release while also minimizing the number of species that must be retained. A time step of 0.1 μs is used and simulations are run for 40 ms to provide sufficient cycles for analysis. All computations are three-dimensional and contain approximately 5 million grid points. Complete details of the simulation procedure can be found in Ref. 17.

C. Power Spectral Density Comparison

The oscillatory pressure-time history of an experimental run in which the length of the oxidizer post was decreased from 7.5 in to 3.5 in is shown in figure 2a. A line showing the oxidizer post length as a function of time is superimposed. The oscillation starts out with a fluctuation of some $\pm$150 kPa and then suddenly jumps substantially above $\pm$400 kPa when the post length reaches 7.2 in indicating a sudden increase in instability characteristics. The magnitude of the oscillation peaks between 5.5 in and 4.75 in, after which the amplitude begins to gradually decrease. By 3.5 in the amplitude of the oscillation is significantly lower.

The contrast between the dramatic jump in amplitude at long post lengths as compared with the gradual transition at short lengths consistently appears in the experimental results as can be seen from figure 2b. This figure shows the variation in the amplitude of the peak power spectral density (PSD) of the first mode as a function of oxidizer post length for various experimental configurations. This is key and shows that the stabilizing mechanisms at play for the 3.5 in and 7.5 in lengths are likely different. Figure 2b indicates that repeating the same test shows that the sudden increase is repeatable. Second, the transition appears not to be affected by the direction of translation. Translating from short to long post lengths produces a similar behavior; a slow and gradual growth of instability after 3.5 in and a dramatic drop in amplitude near the longer length although the transition is delayed from about 6.5 in to 7 in indicating the presence of hysteresis.

Changing the head-end chamber wall conditions also impacts the location of the sharp transition. Replacing the first 5 in of the metal combustor with a quartz/acrylic optical section causes the transition to occur at longer lengths approaching 7.5 in, possibly because the lower thermal conductivity of the optical section results in less heat transfer to the walls. Similarly replacing the first 5 in of the metal combustor with a cooled section causes the transition to occur at shorter lengths, less than 6.5 in. None of these changes, however, has much impact on the PSD amplitudes at other post lengths. The location of transition from

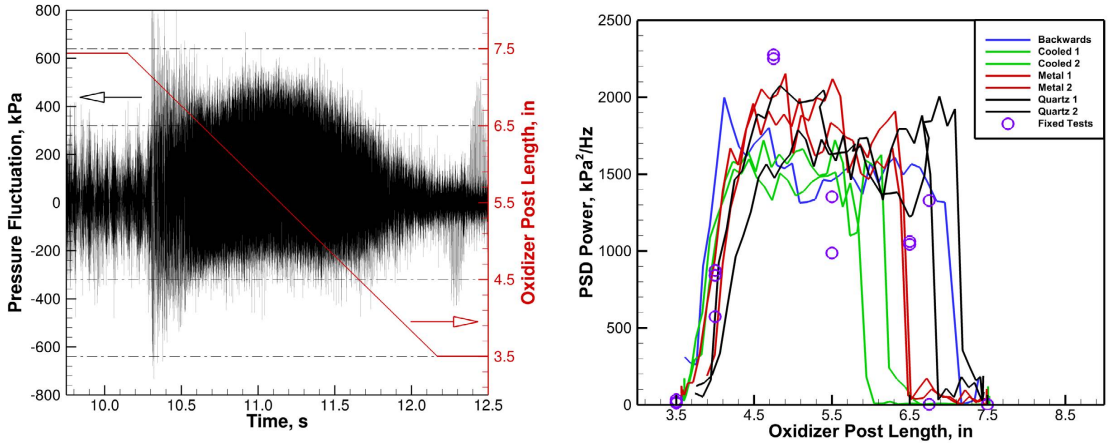

(a) High-pass filtered pressure data from the experiment, plotted with the oxidizer post length. The experiment starts with stable combustion and a length of 7.5 in, as the oxidizer post length is reduced the system becomes unstable. The simulation returns to marginally stable combustion as the post length approaches 3.5 in.

(b) Experimental result for a variety of tests and operating conditions. All translating tests are forward translating with the exception of the single backwards test. Metal, Quartz, and Cooled refer to the treatment of the combustor wall for the first 5 in. Note that the PSD Power is plotted on a linear scale to highlight the variability.

Figure 2: Experimental data

small to large amplitudes is clearly highly sensitive to conditions in the head-end chamber wall conditions, and the location of transition can vary over a range from 6.5 in to 7.5 in.

The spectral content at lengths of 3.5 in, 5.5 in, and 7.5 in for the experiment and simulations are plotted in figure 3. The figure shows PSD analyses for all three lengths. The experimental data were sampled at 0.1 MHz and used a sample size of 160 ms, providing a maximum frequency of 50 kHz and a frequency resolution of 6.25 Hz. Computational PSDs were generated using the final 35 ms of data. The data were sampled at 10 MHz providing a frequency resolution of 28.5 Hz and a maximum frequency of 5000 kHz.

The 3.5 in length has a lower level of instability and only the first two harmonics are clearly distinguishable. Higher modes (if any) are broad. Both the experiment and computation show the defined peaks for the first two modes and broad peaks for the higher modes. It is important not to directly compare the amplitudes of the peaks from the experiment and the computation as it is the area under the peak that determines the power associated with it. A direct comparison can be made by integrating under the PSD peaks. The integration is performed using the full-width half-max (FWHM) method.[10] The peak-to-peak pressure amplitudes as well as the corresponding frequencies for the first three modes are summarized in table 2. The amplitudes of the first three computational modes are in good agreement with the experiment, with the simulations being marginally higher in all three cases. The simulation also shows an additional peak between the first and second mode.

For the unstable 5.5 in length both the experiment and simulation show strong well defined peaks for the first mode as well as the first several harmonics. Amplitudes of the first three modes show excellent agreement with the experiment with the predictions, in this case, being marginally lower.

The quality of the comparison for the 7.5 in length is radically different from the two shorter post lengths. While the experiment records stable combustion, the simulation predicts instability amplitudes similar to those in the 5.5 in case. Clearly, this disagreement may arise from incomplete physics or modeling approximations, but it is also possible that the simulations have yet to transition to stable at this post length. The 7.5 in post length is near the experimentally observed transition in disturbance amplitude which was shown to be sensitive to the direction of translation and the wall heat flux. For example, the adiabatic wall assumption in the simulations should move the transition to longer post lengths. Possible reasons for the unstable behavior are discussed in the Cycle Analysis section where it is also argued that the driving

mechanisms in the 5.5 in and 7.5 in lengths are different despite their similar amplitudes.

Predicted frequencies are high but follow the same trend, decreasing frequency with increasing oxidizer post length. The higher frequency may be the result of the simplified chemical kinetics and/or adiabatic wall boundary conditions, both of which result in higher sound speeds than the experiment. The mean pressure is also higher in the simulation, 1.5 MPa compared to 1.3 MPa in the experiment which suggests that the combustion may not be complete in the experiment.

The ratios of the frequencies of the higher-order modes to the first mode are in excellent agreement with the experiment for the 3.5 in and 5.5 in cases; both predict near integer multiples of the frequency. The exception to this is the third mode of the 3.5 in case for which both simulation and experiment predict non-integer multiples, the ratio is however somewhat different between the two. Ratios are tabulated in table 2.

Table 2: Frequency and peak-to-peak pressure amplitudes for the experimental and computational operating points.

Oxidizer Post Length, in	Mode	Experiment			Simulation		
		f, Hz	p'_{ptp}, kPa	f_i/f_1	f, Hz	p'_{ptp}, kPa	f_i/f_1
3.5	1	1379	121.17	1.00	1720	133.04	1.00
	?	–	–	–	2720	40.33	1.58
	2	2734	5.86	1.98	3400	19.15	1.98
	3	3882	16.03	2.82	4400	22.32	2.56
5.5	1	1324	387.15	1.00	1571	308.68	1.00
	2	2655	89.29	2.01	3114	85.11	1.98
	3	3979	46.37	3.01	4685	43.25	2.98
7.5	1	1220	15.57	1.00	1486	395.84	1.00
	2	3650	8.10	2.99	3000	158.23	2.02
	3	–	–	–	4486	73.25	3.02

III. Identification of Instability Mechanisms

This section identifies three phenomena that occur in the computational (and experimental) results that appear to impact instability characteristics present in the CVRC. The relative timing between pressure pulses and key events is clearly important in elucidating instability mechanisms. Accordingly we first start by providing "back of the envelope" estimates of the traverse times of pressure pulses in the combustor and oxidizer post. The second phenomenon is the role of vorticity production by baroclinic torque, while the third is the transitory migration of tribrachial flames.

A. Pulse Timing

Table 3 lists estimated mean values for the velocity and sound speed along with the relevant lengths of the combustor and oxidizer post. These quantities are are then used with simple acoustic theory to estimate the travel times of pressure pulses to help anchor the events in the simulations. The travel times are estimated using,

$$\begin{aligned} t &= t^{\Rightarrow} + t^{\Leftarrow} \\ t &= \left(\frac{L}{c+u}\right) + \left(\frac{L}{c-u}\right). \end{aligned} \tag{1}$$

where L is the length, c is the sound speed, and u is the mean velocity. The downstream travel time is denoted by $t^{\Rightarrow}$ and the upstream travel time is $t^{\Leftarrow}$. The effect of mean flow is considered because of the high velocity in the oxidizer post relative to the sound speed. For consistency this assumption, although less

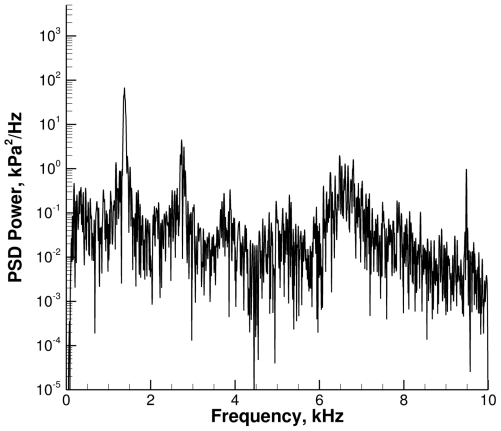

(a) 3.5 in, Experiment.

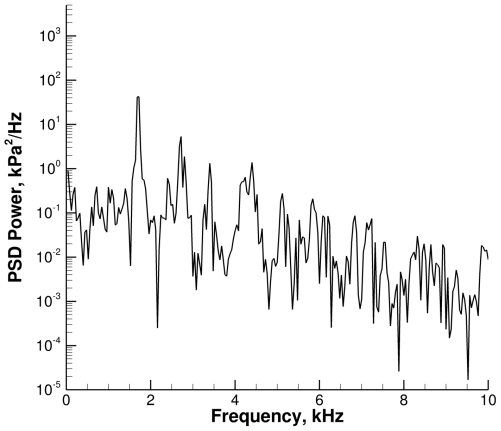

(b) 3.5 in, Simulation.

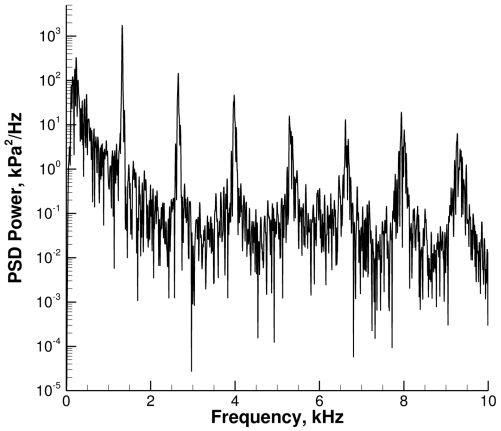

(c) 5.5 in, Experiment.

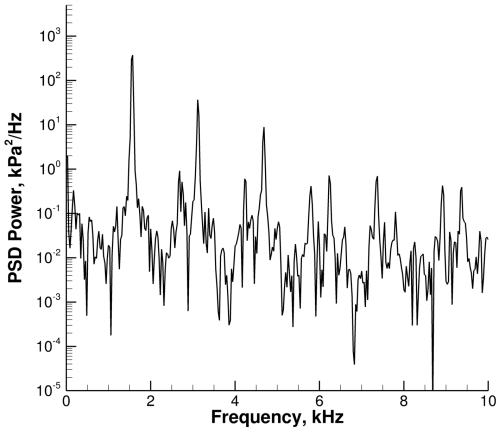

(d) 5.5 in, Simulation.

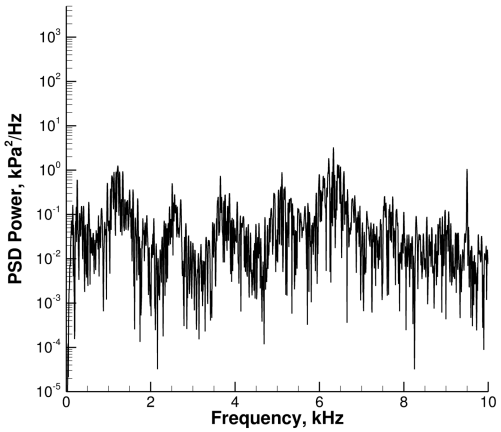

(e) 7.5 in, Experiment.

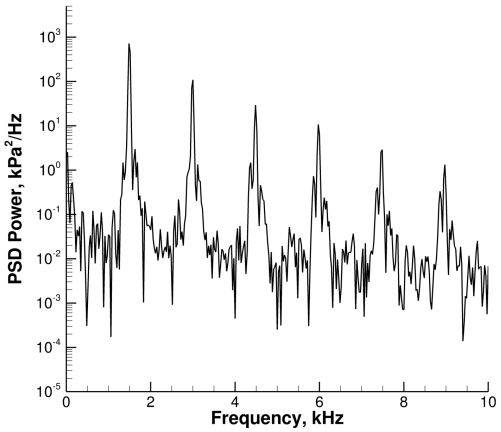

(f) 7.5 in, Simulation.

Figure 3: PSD analysis for the experimental (left) and simulations (right). Point of analysis is 14.5 in downstream from the backstep.

important, is also carried through for the combustor analysis. Absent from this analysis is the pressure rise due to combustion.

Table 3: Approximate pulse times from a simple acoustic analysis.

Region	Parameter	3.5 in (8.89 cm)	5.5 in (13.97 cm)	7.5 in (19.05 cm)
Combustor	L		38.1 cm	
	u		16.0 cm/ms	
	c		120.0 cm/ms	
	$t^{\Rightarrow}$		0.28 ms	
	$t^{\Leftarrow}$		0.37 ms	
	t		0.65 ms	
	$f = c/2L$		1574 Hz	
Ox Post	L	8.89 cm	13.97 cm	19.05 cm
	u		22.0 cm/ms	
	c		69.0 cm/ms	
	$t^{\Rightarrow}$	0.10 ms	0.15 ms	0.21 ms
	$t^{\Leftarrow}$	0.19 ms	0.30 ms	0.40 ms
	t	0.29 ms	0.45 ms	0.61 ms
	$f = c/2L$	3880 Hz	2470 Hz	1811 Hz

As the oxidizer post length is varied, the wave transit times in the post change while those in the combustor remain constant leading to different matching. Therefore, a combustor pressure pulse starting from the backstep will encounter different conditions when it returns for every change in the oxidizer post length. A cycle starts and ends at the same point in the combustor, with high pressure at the backstep. Figure 4 is a sketch showing the pulse movements for a single cycle for the three cases. The wave movements were constructed using the transit times listed in table 3.

The timing of the pressure pulse in the oxidizer post is different for each of the three cases. When the pulse returns from the oxidizer post and the pressure in the combustor is low the pulse expands radially outward into the combustor. This radial expansion forces any fuel in the shear layer outward into the recirculation region where hot gasses are present. This event has the potential to cause ignition near the backstep. In the case where the combustor pressure is not low at the time of the returning pulse, the event appears to be insignificant. For the 5.5 in length the return time of the pulse is coincides with the lowest pressure point of the cycle. This is not the case for the 3.5 in or 7.5 in lengths. Instead for the 3.5 in case the return wave coincides with the falling chamber pressure before significant fuel can accumulate. In the 7.5 in case the wave returns after the pressure in the combustor begins to increase.

B. Baroclinic Torque

Increased mixing can give rise to higher combustion heat release. One source of increased mixing is an increase in vorticity in regions of non-premixed flow. To understand the sources of vorticity we look to the vorticity transport equation. For compressible flow with no body forces the equation describing vorticity is,

$$\frac{\mathrm{d}\boldsymbol{\omega}}{\mathrm{d}t} = (\boldsymbol{\omega}\cdot\nabla)\,\mathbf{u} - \boldsymbol{\omega}\,(\nabla\cdot\mathbf{u}) + \frac{1}{\rho^2}\,(\nabla\rho\times\nabla p) + \nabla\times\left(\frac{1}{\rho}\nabla\cdot\boldsymbol{\tau}\right). \tag{2}$$

The term of interest is the baroclinic torque, which is the third term on the right hand side. This term represents the generation of vorticity due to density and pressure gradients that are misaligned.[34] The region near the fuel injection is home to strong density gradients where the cold dense fuel sits adjacent to the warm less dense oxidizer. Consider the sketch of a shear layer shown in figure 5. As the pressure pulse moves (upstream or downstream) through the oxidizer post the pressure gradient is aligned with the axial direction and there is a strong radial density gradient. This configuration will result in a generation

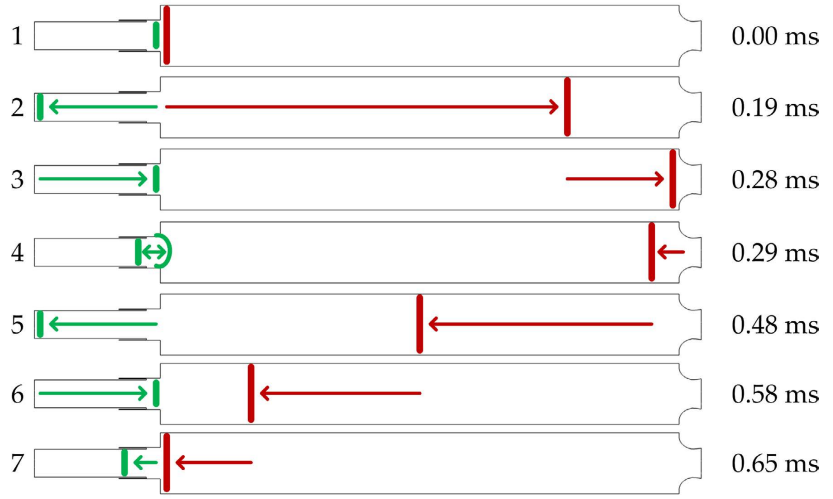

(a) 3.5 in.

(b) 5.5 in.

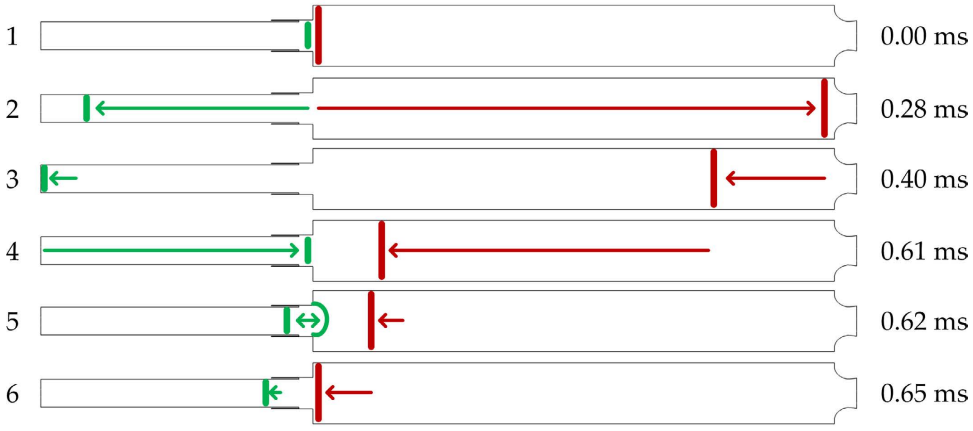

(c) 7.5 in.

Figure 4: Acoustic wave events. Times to the left are the elapsed time of the cycle.

Figure 5: Shear layer showing the dense fuel against the wall and the less dense oxidizer in the core.

of vorticity in the circumferential direction. Vorticity generation in this region can promote mixing of the oxidizer and fuel resulting in portions of the flowfield that are partially premixed. These partially premixed regions can result in combustion taking place upstream of the backstep.

C. Tribrachial Flame

A tribrachial flame, also called a triple flame, is the result of three combustion phenomena occurring at a single point. At this point (or line in three-dimensions) there is a fuel rich premixed flame, fuel lean premixed flame, and a diffusion flame.[35] This point, often referred to as a triple point or tribrachial point, is a location of intense heat release. Identification of the tribrachial flame is possible by exploring the local mixture fraction. The mixture fraction is defined as,[36]

$$\mathsf{Z} = \frac{\nu_{\text{st}} Y_{\text{CH}_4} - Y_{\text{O}_2} + Y^0_{\text{O}_2}}{\nu_{\text{st}} Y^0_{\text{CH}_4} + Y^0_{\text{O}_2}} \tag{3}$$

where $\nu_{\text{st}} = 4.0$, $Y^0_{\text{CH}_4} = 1.0$, and $Y^0_{\text{O}_2} = 0.4235$ for the present configuration. Also relevant is the stoichiometric mixture fraction, $\mathsf{Z}_{\text{st}} = 0.095739$. Figure 6 shows snapshot of the triple flame structure from the present simulations. There are three distinct layers, comprising oxidizer, fuel, and the burnt gases in the recirculation region. Garby et al. also deduced the existence of the triple flame structure using a simulation for an unstable 4.75 in case. They suggest that no burning occurs upstream of the backstep and the hot recirculation gases are responsible for heating the mixture of unburnt fuel and oxidizer. They note that the chemistry is not fast enough to anchor the flame at the injection point and the flame is instead anchored at the dump plane by the hot burnt gases in the recirculation region.[21] Guézennec et al. showed that in an unstable 4.75 in case the triple flame forms at the backstep and is extinguished when it hits the wall, the time of this movement is linked to the first longitudinal mode.[22] Results in this work find that the mechanism at play in the unstable case is more complex and dynamic. The triple flames move throughout the head-end of the combustor. They are extinguished and reform regularly and in some instances can be found upstream of the backstep.

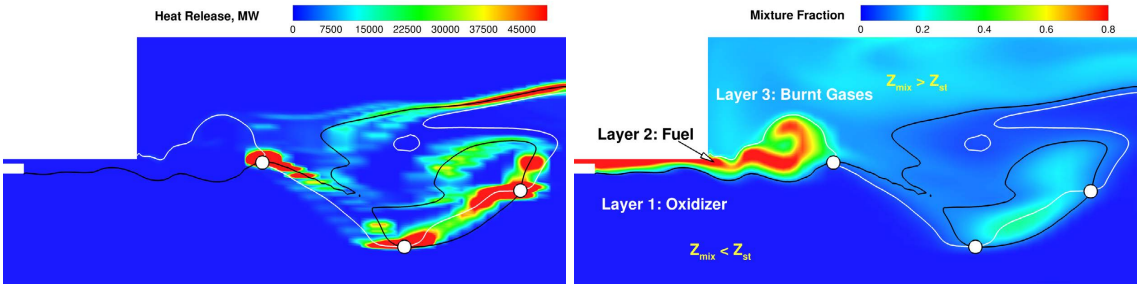

(a) Intense heat release at the triple points.

(b) Mixture fraction showing the three layers.

Figure 6: Tribrachial Flame structure, three tribrachial points are identified (white circles) at the intersection of the white and black lines. In both plots the white line is a $T = 2000\,\text{K}$ contour and the black line is the stoichiometric mixture fraction, Z_{st}.

IV. Cycle Analysis

The following three sections look at the behavior of the three oxidizer post lengths for a single cycle. The elements of instability presented in the previous section are highlighted. Figure 7 shows the cycles that will be examined for each case. Six points are marked on each cycle, these points have been judiciously chosen to highlight the events discussed in the above section as well as illustrating the overall unsteady behavior. The results for the 5.5 in length are presented first, the remaining two lengths build on the 5.5 in results.

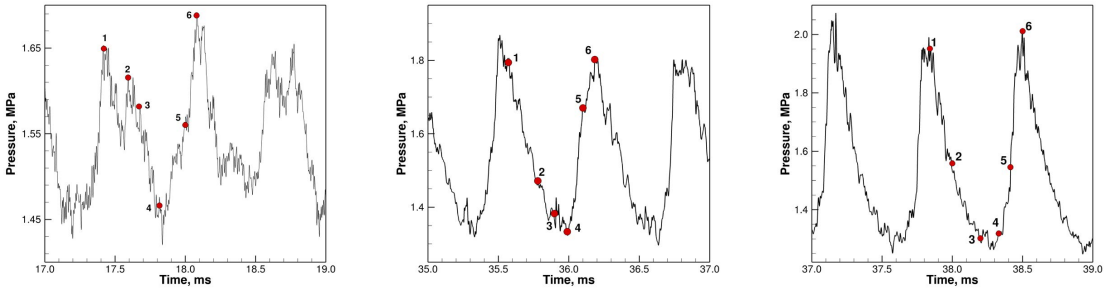

(a) 3.5 in. (b) 5.5 in. (c) 7.5 in.

Figure 7: Pressure plots of the cycle of interest for each configuration. Note that the pressure scales are different in each figure.

A. 5.5 in Oxidizer Post Length

The time varying pressure near the backstep is shown in figure 7b. Although the instantaneous flowfield is three-dimensional, sufficient understanding and improved visualization can be realized from two-dimensional slices. Figure 8 shows a series of plots for the six points in the cycle marked in figure 7b. The plots on the left are of the CH_4 contour, superimposed on the contour are lines colored with the static pressure. Plots on the right are of a combustion heat release contour, two lines are superimposed on the contour, the white line signifying a temperature of 2000 K a black line marking the stoichiometric mixture fraction allowing for triple flame identification.

Starting at point one, the cycle has just begun and the pressure in the combustion region is decreasing. The pressure shows that there are two pulses moving away from the backstep in opposite directions, one moving upstream in the oxidizer post and a second moving downstream in the combustor. The CH_4 mass fraction shows disrupted flow near the injection, this is the result of the pressure pulse that moved upstream in the oxidizer post. The combustor is largely absent of any significant concentrations of CH_4 with the exception of an annular region near the wall close to the impingement point of the primary recirculation region. The temperature line serves to demarcate the burnt and unburnt gases; combustion along the temperature line is due to a diffusion flame. There is significant heat release before the backstep adjacent to the wall in the region where CH_4 is absent. Significant heat release in the combustor is confined to the region near the temperature line and the annular pocket of CH_4 near the impingement point. Triple points are located away from the backstep.

As the cycle progresses to point 2 the pressure continues to drop. The distribution of CH_4 is very different from the last time, there are significant concentrations of CH_4 past the backstep in the shear layer. Looking at the heat release, we can see that this region is not combusting. Also note that there is no longer any combustion upstream of the backstep despite the high concentrations of CH_4 lining the wall. This region is no longer sufficiently premixed to support combustion. The region where the fuel is located is lower in temperature; the stoichiometric line and temperature line are further apart in regions where there is no burning. Also, note that unlike the previous time the burning here is concentrated in the center of the combustor not near the walls. The triple point holds roughly the same axial position as the previous time.

Point 3 sits in the trough of the cycle, just before the incoming pressure pulse in the oxidizer post returns to the combustor. There is significant CH_4 in the combustor along the shear layer. An accumulation of fuel is present near the combustor wall. This results from fuel being pulled out of the shear layer by the

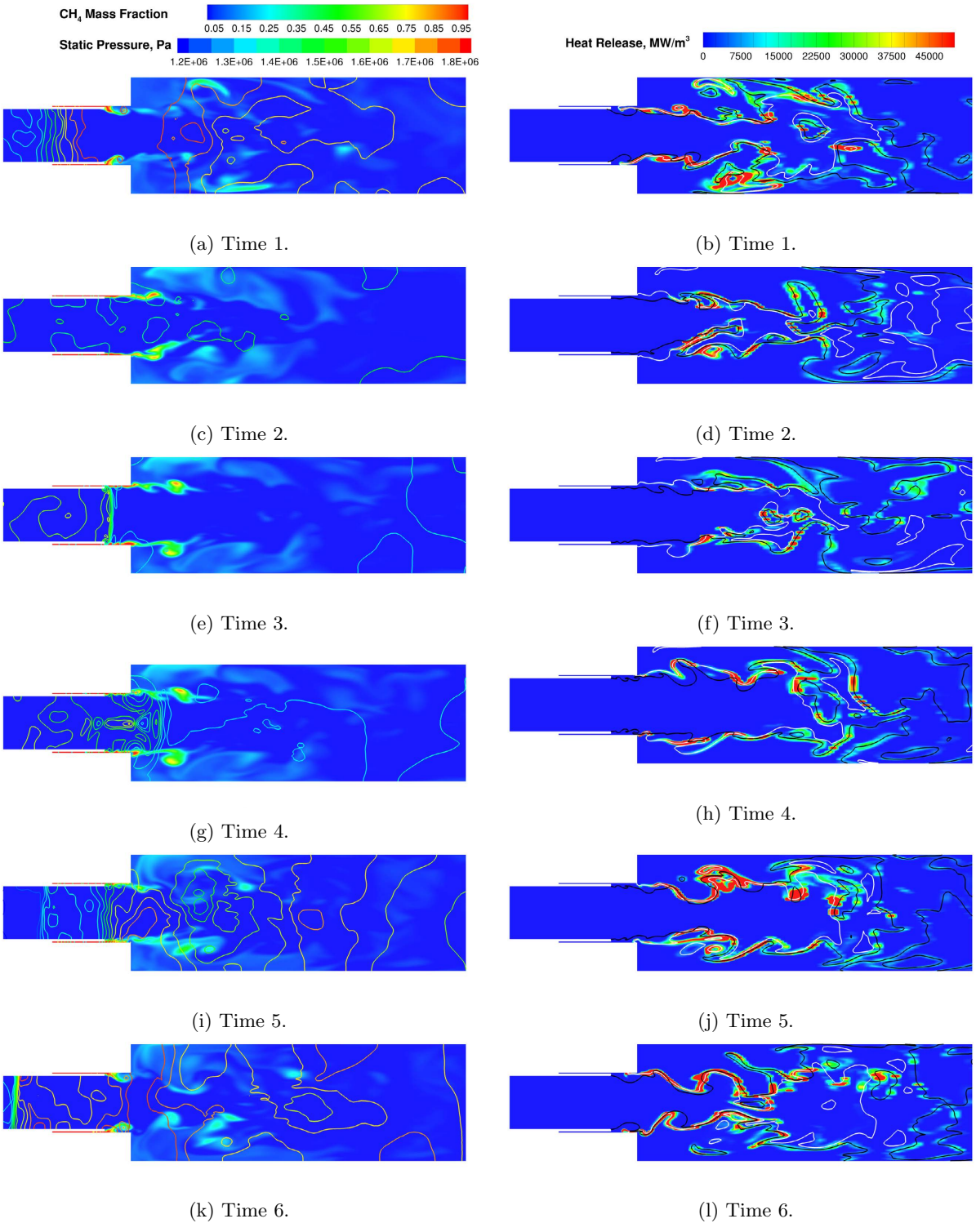

(a) Time 1.

(b) Time 1.

(c) Time 2.

(d) Time 2.

(e) Time 3.

(f) Time 3.

(g) Time 4.

(h) Time 4.

(i) Time 5.

(j) Time 5.

(k) Time 6.

(l) Time 6.

Figure 8: Cycle snapshots for 5.5 in. Left images: contour is colored with CH_4 mass fraction, lines are colored with static pressure. Right images: contour is colored with combustion heat release, the white lines are a temperature iso-line for $T = 2000\,\mathrm{K}$, and the black line represent the stoichiometric mixture fraction. Contour levels are consistent for all times.

recirculation region. The heat release contours show that these regions of high fuel concentration are not burning. The triple points have moved further downstream along with the significant heat release.

In the oxidizer post, the pressure pulse is just passing the fuel collar and moving downstream towards the combustor. As the pressure pulse passes through the fuel injection region generates vorticity in this area because of a non-zero baroclinic torque. This creates a partially-premixed region upstream of the backstep allowing combustion to take place in this region at a later time. The effect of the baroclinic torque for all three lengths is contrasted following the cycle analysis.

When the pressure pulse passes the backstep and moves into the combustor there is a spike in pressure visible in the wave trough (figure 7b). A plot of the flowfield at this time is shown in figure 9. This figure shows the pressure wave expanding into the combustor. As it moves into the combustor it expands radially outward pushing the CH_4 rich fluid into the hot recirculating gases. Although not shown there is no heat release occurring in the region of high CH_4 concentration.

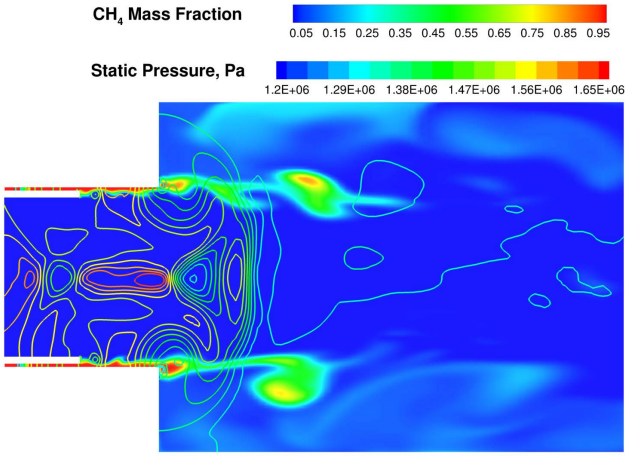

Figure 9: Snapshot at the trough of the wave just past point 3. Close up showing the radial displacement of the fuel near the backstep. Contour is colored with CH_4 mass fraction, lines are colored with static pressure.

Point 4 in the cycle represents the final low pressure point. Notice that flame is now attached to the wall, figure 8h. Flame attachment is due to the pressure wave in the oxidizer post pushing the fuel oxidizer mixture outward into the recirculation region. The recirculation region has hot combustion products and this parcel of fuel and oxidizer ignites very close to the wall, this flame then propagates back to the wall (and in some instances upstream of the backstep) along the wall due to the partially premixed region present (created by the previously passing pulse from the baroclinic torque).

The ignition of methane near the backstep is responsible for the rapid pressure increase that occurs after point 4. There is a large increase in pressure as we move from point 4 to 5, almost 0.4 MPa. This is not due to any pressure pulses. The pulse in the combustor is on its way back to the backstep but has not yet arrived and the pressure pulse in the oxidizer post largely dissipates after expanding into the combustor between points 3 and 4. This pressure rise is the result of the combustion in the region. In the snapshot for time 5 the pressure pulse moving upstream towards the backstep.

By time six, the high-pressure pulse resulting from combustion has begun to propagate upstream in the oxidizer post. The upstream propagating pressure wave disrupts the incoming fuel flow; notice the elevated concentrations of methane away from the wall. The absence of methane close to the wall is the result of combustion in that region completely consuming the fuel before it enters the combustor. The combination of this burning and the flow disruption will act to starve the combustor of fuel at the beginning of the next cycle. This sets up the extinction event that occurs shortly after the start of the cycle, allowing the heat release to move downstream.

B. 3.5 in Oxidizer Post Length

The computations and experimental results show that the 3.5 in oxidizer post length is marginally stable, having peak-to-peak amplitudes of about 150 kPa compared to the 600 kPa amplitudes of the 5.5 in case.

There are key several differences to the story presented for the 5.5 in case. The first notable difference is the continuous behavior of the heat release in the combustor. This continuous heat release is possible because the starvation event that occurred in the 5.5 in case is absent; instead fuel is continuously fed into the combustor. The heat release still couples with the pressure to some degree but the large reignition event which results from the accumulation of unburnt fuel is absent in the combustor. A pressure trace for the cycle of interest was shown in figure 7a. The lower amplitudes result in cycles that are not as regular, but the chosen cycle is representative of the overall limit cycle behavior.

A plot of snapshots for the cycle is shown in figure 10. Note that for this case the pressure amplitudes are much lower and tend to show more variability in the radial direction. There is no heat release upstream of the backstep along the wall and there is no disruption to the fuel flow from the high-pressure pulse moving through the oxidizer post. These are two immediate differences from the 5.5 in case. Triple points are located downstream of the backstep.

Moving to point two, there is a second relative peak in the pressure signal near the backstep. This peak is the result of continued combustion in the region. The initial decay from point 1 is the result of the acoustic waves moving away from the backstep towards the nozzle and oxidizer injector. Without the starvation event, the combustion continues and the pressure briefly increases. At time 2 there is unburnt fuel in the combustor near the backstep but for the majority of the combustor there is a diffusion flame positioned along the $T = 2000\,\mathrm{K}$ line. In the instant shown this flame extends upstream almost reaching the backstep. In this instance, a triple point is located near the backstep (top of the figure).

The pressure pulse in the oxidizer post returning to the combustor is a non-event in this case, occurring at point 3. The travel time for the wave is much faster but the frequency of the first longitudinal mode is not that different from the 5.5 in length. This results in the pulse returning while the head end pressure is still decreasing. The smaller pressure gradient results in less vorticity generated from the baroclinic torque. The result is less mixing of the fuel and oxidizer in the shear layer upstream of the backstep preventing combustion from occurring before the backstep by not creating a region sufficiently premixed to support combustion. There is heat release close to the backstep which extends downstream along the $T = 2000\,\mathrm{K}$ line. Recall that in the 5.5 in case the starvation of fuel led to a absence of heat release adjacent to the backstep as the pressure decreased to the low point of the cycle.

Time 4 is the low pressure point of the cycle. Heat release continues near the backstep with combustion again primarily taking place along the $T = 2000\,\mathrm{K}$ line which is offset from the stoichiometric mixture fraction line. There is no heat release upstream of the backstep. The lack of combustion upstream of the backstep continues as the pressure increases. At time 5 the returning high pressure pulse is visible at the downstream end of the viewing region.

When the head end of the combustor returns to the high pressure point there is the largest amount of heat release. The flame is again primarily located along the $T = 2000\,\mathrm{K}$ line with peak heat release near the intersection of the temperature and mixture fraction lines. There is no combustion before the backstep and the fuel adjacent to the wall in the oxidizer post does not show any disruptions from the passing pressure pulse. These two factors allow for the continuous flow of fuel into the combustor for the next cycle eliminating the reignition event.

C. 7.5 in Oxidizer Post Length

The simulation for the 7.5 in case does not agree with the experimental results predicting unstable combustion instead of the observed stable behavior. At the present time it is unknown why this is the case. The experimental result is very close to the stability margin and it is likely that the simulations are missing the boundary. Possible reasons include an incorrect frequency, which would adjust the wave timing and the use of adiabatic walls, which do not allow heat to be lost through the combustor walls. Despite this result it is worthwhile to go through the cycle analysis because there are differences between the 5.5 in and 7.5 in cases. A pressure plot showing the points of analysis was shown in figure 7c.

Figure 11 shows the flowfield over the cycle of interest. Similar to the 5.5 in length the beginning of the cycle shows disrupted fuel near the inlet and combustion taking place upstream of the backstep. The pressure pulse that moves into the oxidizer post from the combustor is responsible for pushing the incoming fuel backwards. This pulse also generates vorticity though the baroclinic torque which results in a region upstream of the backstep, which is partially premixed. One difference is the presence of a triple point (line) upstream of the backstep, this was not observed for either the 3.5 in or 5.5 in length.

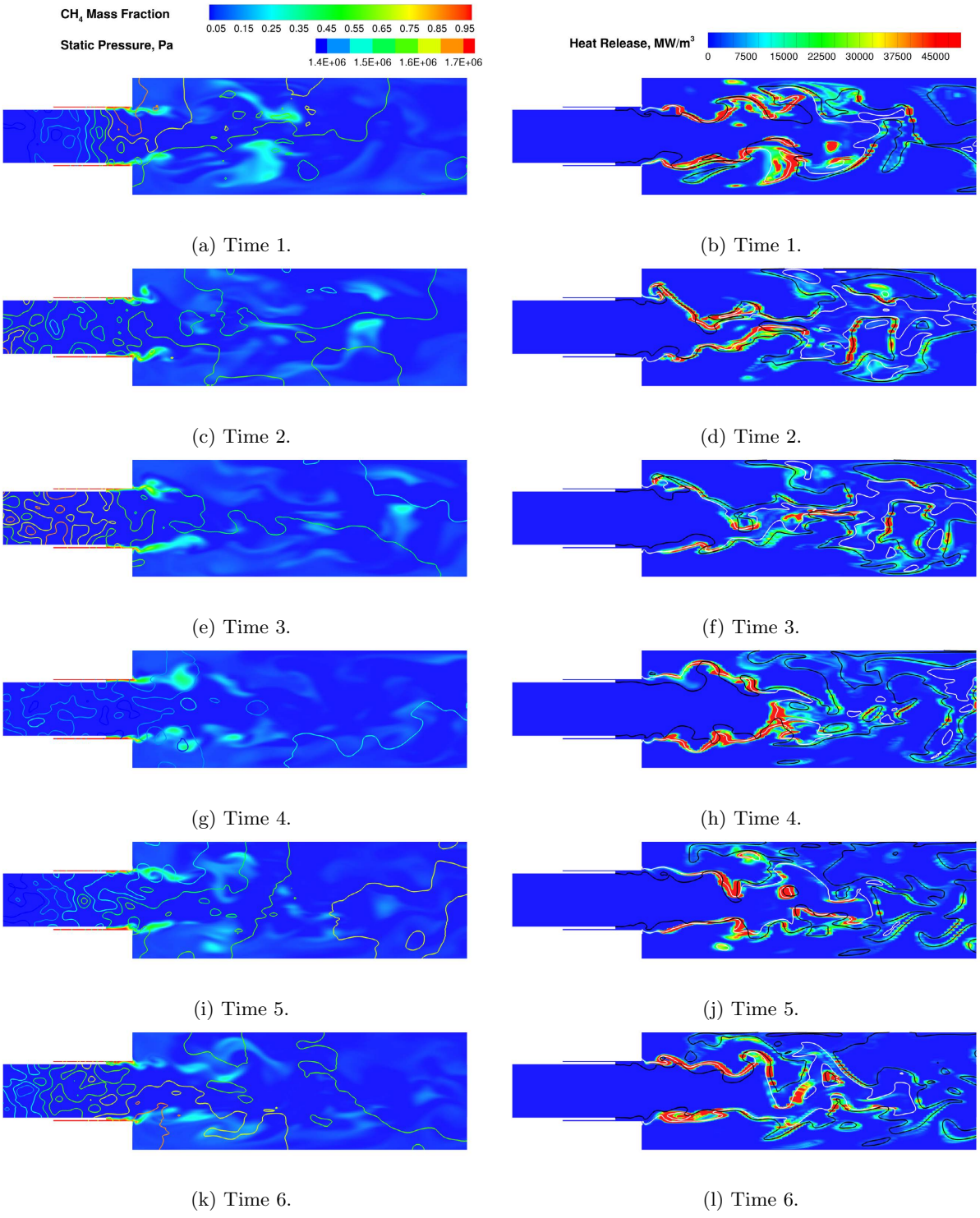

(a) Time 1.

(b) Time 1.

(c) Time 2.

(d) Time 2.

(e) Time 3.

(f) Time 3.

(g) Time 4.

(h) Time 4.

(i) Time 5.

(j) Time 5.

(k) Time 6.

(l) Time 6.

Figure 10: Cycle snapshots for 3.5 in. Left images: contour is colored with CH_4 mass fraction, lines are colored with static pressure. Right images: contour is colored with combustion heat release, the white lines are a temperature iso-line for $T = 2000\,\mathrm{K}$, and the black line represent the stoichiometric mixture fraction. Contour levels are consistent for all times.

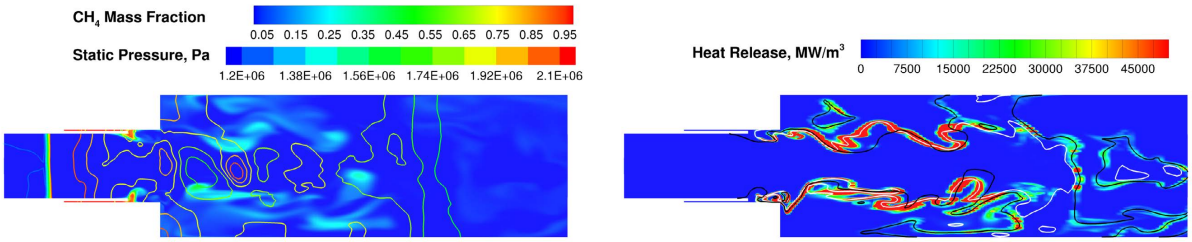

(a) Time 1.

(b) Time 1.

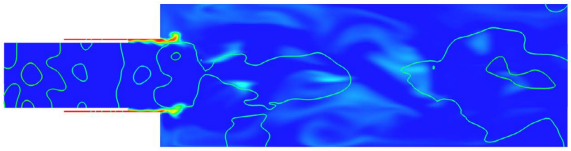

(c) Time 2.

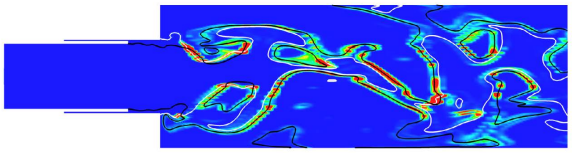

(d) Time 2.

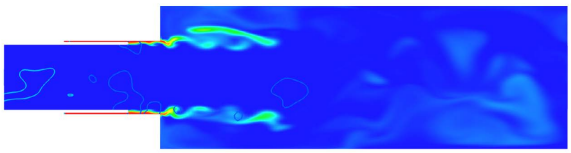

(e) Time 3.

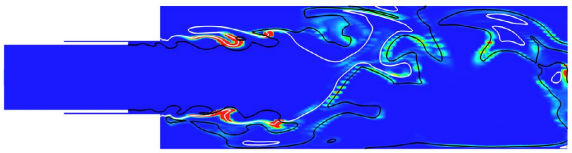

(f) Time 3.

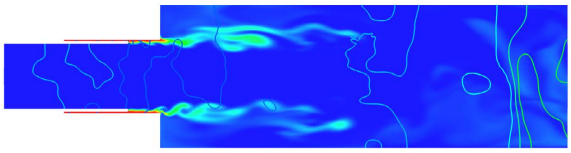

(g) Time 4.

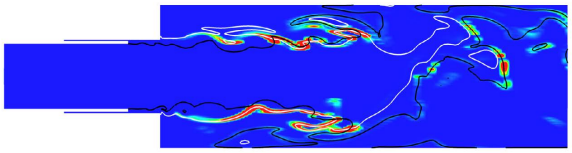

(h) Time 4.

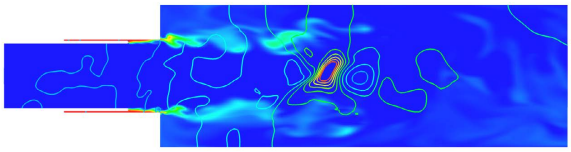

(i) Time 5.

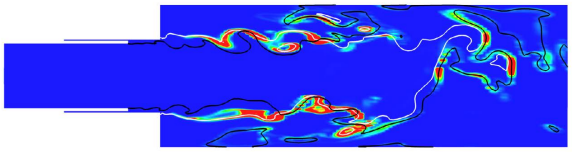

(j) Time 5.

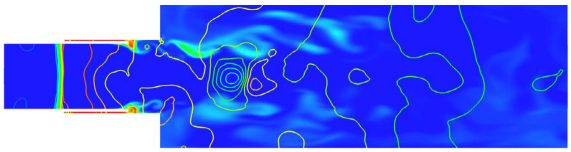

(k) Time 6.

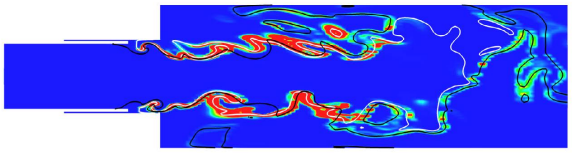

(l) Time 6.

Figure 11: Cycle snapshots for 7.5 in. Left images: contour is colored with CH_4 mass fraction, lines are colored with static pressure. Right images: contour is colored with combustion heat release, the white lines are a temperature iso-line for $T = 2000\,\mathrm{K}$, and the black line represent the stoichiometric mixture fraction. Contour levels are consistent for all times.

As the pressure decreases, time 2, the triple point moves downstream and combustion upstream of the backstep stops. This is due to the flow disruption and depletion of partially premixed fluid in the region. Fuel begins to accumulate at the dump plane. By the trough of the wave, point 3, there is significantly less heat release in the combustor and the shear layer has a high concentrations of CH_4. CH_4 is also found in the recirculation region. Heat release is primarily taking place along the temperature isoline (diffusion flame).

For the 7.5 in length the returning oxidizer post wave does not appear in the trough of the wave. Time 4 is just before the pressure in the combustor begins to rise. In the combustor CH_4 concentrations are elevated. These fluid parcels with elevated CH_4 concentration can be found further downstream than was observed in either the 3.5 in or 5.5 in cases. The downstream fuel is warmed from the adjacent hot recirculation gases. This is evident by the stoichiometric line sitting outside the temperature isoline. The now warm fuel begins to combust producing an annular ring of significant heat release. At time 5 there is a localized pressure rise located at the center of the burning annulus (figures 11i-11j). Note that at this late stage in the cycle the flame is not yet attached to the backstep and there is no burning upstream of the backstep instead combustion is taking place downstream. This point is when the oxidizer post wave returns; its return however is overshadowed by the large pressure rise in the combustor from the downstream heat release.

At the end of the cycle, there is substantial heat release along the shear layer extending back into the oxidizer post. Again, note the presence of the triple point near the fuel injection. The fuel being consumed near the injector will give rise to the starvation event for the next cycle. For the 7.5 in case reignition after the starvation event is due to fuel in the combustor warming next to the recirculation gases downstream. For the 5.5 in case the reignition was due to the returning wave pushing the fuel into the recirculation gases at the backstep. This suggests that the effect of wall temperature in this region may be important in accurately predicting the stability at this length.

D. Baroclinic Torque

Vorticity generation in the shear layer upstream of the backstep through the baroclinic torque occurs when a pressure pulse passes through the region. Increased vorticity leading to increased mixing generates a partially-premixed region of fuel and oxidizer upstream of the backstep that is susceptible to combustion. Combustion upstream of the backstep is a precursor for the starvation event, which ultimately leads to the instability. Figure 12 shows the baroclinic torque in the vicinity of the backstep for the three oxidizer post lengths. The snapshots are taken just after the oxidizer pressure pulse passes through the region. Notice that in the 3.5 in case which does not show the starvation event there is significantly less vorticity being generated compared to the 5.5 in and 7.5 in cases which do exhibit the starvation event. The presence of the partially-premixed region upstream of the backstep allows for combustion to take place in this region. Recall that in the case of the 3.5 in length no combustion was found upstream of the backstep.

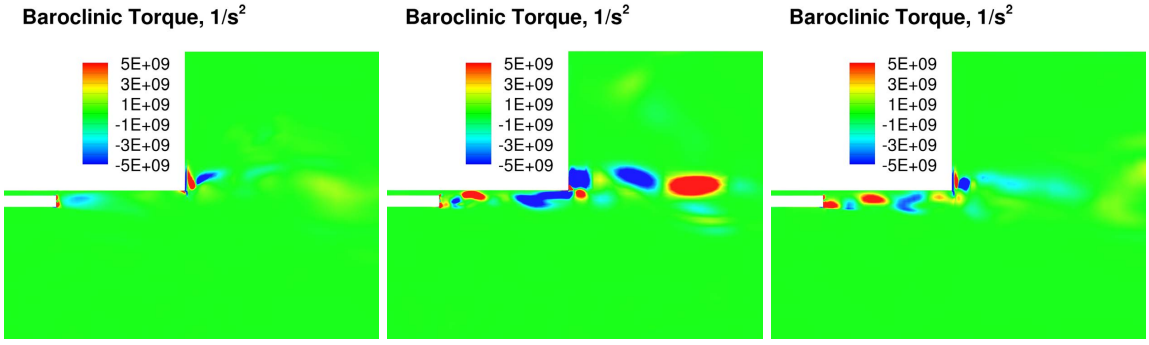

(a) 3.5 in. (b) 5.5 in. (c) 7.5 in.

Figure 12: Baroclinic torque near fuel injector. Snapshot shows the time just after the pressure pulse passes by the region.

E. Rayleigh Index

As a final assessment of the effect of post length on instability, we compare Rayleigh indices[37] for the three different post lengths. The Rayleigh index provides a measure of the correlation between pressure and combustion heat release oscillations and is often cited as an instability mechanism. To obtain local values of the index over the active combustion area, we integrate over each individual cell volume using the mathematical expression,

$$\mathscr{R}(\mathbf{x}_i) = \frac{1}{T}\int_{t_0}^{t_0+T} p'(\mathbf{x}_i,t)\dot{q}'(\mathbf{x}_i,t)\,\mathrm{d}t. \tag{4}$$

Representative results are summarized in figure 13. For all three post lengths, areas of non-zero Rayleigh index appear in the region downstream of the backstep. Positive values (indicating regions where the pressure and heat release are in phase and amplify the instability) arise in the shear layer, while negative values (representing out of phase regions which damp the instability) appear in the recirculation region and, for the two longer post length cases, near the center line. Surprisingly, the Rayleigh index downstream of the backstep, suggests the relatively stable 3.5 in case has the strongest driving (although it also appears to have stronger regions of damping), while the highly unstable 5.5 in length exhibits the weakest growth.

In the small region upstream of the backstep where combustion was observed for the two longer post-length cases the 3.5 in case shows neither positive nor negative Rayleigh indices in agreement with the previously noted absence of combustion upstream of the backstep for this case. The Rayleigh index for the 5.5 in and the 7.5 in cases is relatively strong in this region, and extends nearer to the splitter plate in the latter case, possibly explaining the reasons for the stronger instability in these two simulations. Overall, the Rayleigh index results are somewhat puzzling and further work is needed to interpret their meaning. It has been suggested by Nicoud and Poinsot that it is the fluctuating energy equation (which accounts for entropy) not the standard acoustic energy equation that should be used for the analysis of turbulent combustion. They also state that the Rayleigh index must be compared against the acoustic losses at the boundary, not zero.[38] The results of this work appear to demonstrate that the standard Rayleigh index is not the be-all and end-all tool for stability analysis.

V. Summary

Simulations of the CVRC experiment were performed at three discrete lengths, which encompass the three stability regimes of the experiment, marginally stable, unstable, and stable. Simulations are able to replicate the marginally stable 3.5 in length and the unstable 5.5 in length but fail to predict stability for the 7.5 in length. In the marginally stable case, the cycle analysis revealed that the heat release is continuous leading to overall less unsteadiness. The resulting pressure fluctuations have lower amplitudes, pressure pulses traveling in the oxidizer post are not strong enough to disrupt the incoming fuel or generate fluid that is sufficiently premixed to allow combustion upstream of the backstep. In the absence of these two events fuel flows into the combustor continuously. The timing of the return wave in the oxidizer post coincides with the falling pressure in the combustor and is a non-event.

In the unstable 5.5 in case the heat release is cyclic. The cyclic heat release is the result of a fuel starvation event. The starvation event is a result of the pressure pulse in the oxidizer post disrupting the incoming fuel flow and generating a partially premixed region through the baroclinic torque. When this partially premixed region combusts, it consumes all of the available fuel and cuts off the supply into the combustor. The temporary starvation of fuel allows combustion to move downstream away from the backstep. As the fuel supply is reinitiated, the lack of heat release at the head-end allows for fuel to buildup in the combustor. The returning wave in the oxidizer post expands into the combustor at the low pressure point of the cycle. In doing so, the accumulated fuel in the shear layer adjacent to the backstep is pushed into the hot gasses in the recirculation region. This results in a massive reignition event with a rapid increase in pressure. The rapid increase in pressure coincides with the returning acoustic wave in the combustor. The large amplitude pressure disturbance then travels into the oxidizer post and triggers the starvation event.

The unstable 7.5 in case does not follow the same pattern as the 5.5 in case. While there is a starvation event that is due to the same mechanism as the 5.5 in case the subsequent reignition event is due to a different mechanism. Because of the longer post length the returning ox-post wave does not arrive a low pressure point of the cycle instead arriving when the combustor pressure is already increasing. The reignition even instead occurs further downstream as the massive amount of fuel in the combustor slowly mixes with the

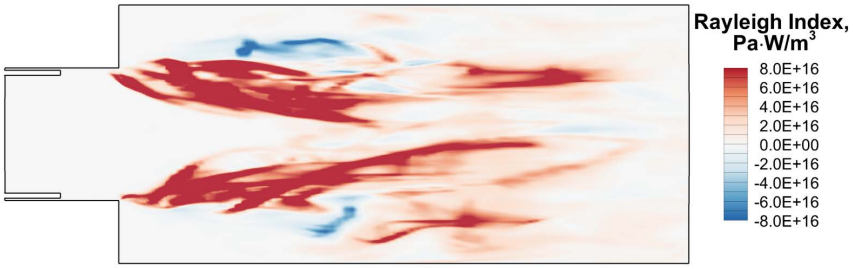

(a) 3.5 in.

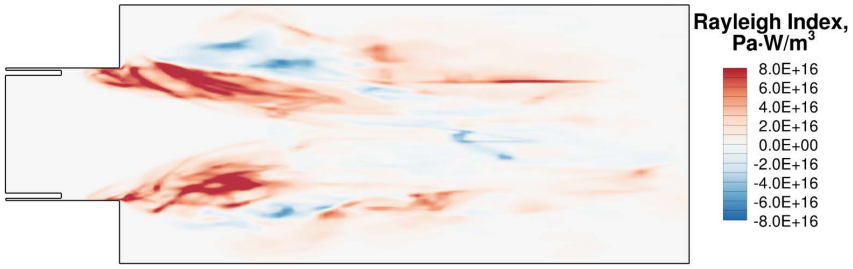

(b) 5.5 in.

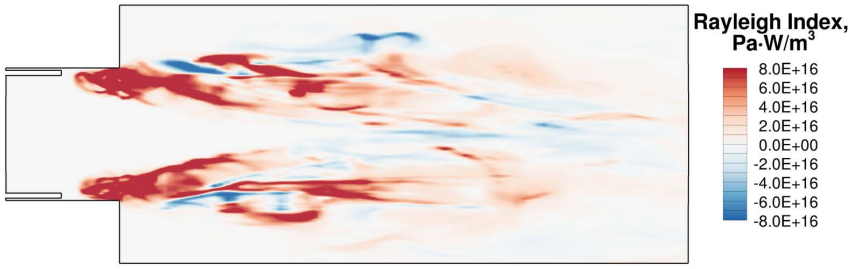

(c) 7.5 in.

Figure 13: Rayleigh index. The region shown starts 3 cm upstream of the backstep and extends 10 cm downstream of the backstep.

hot recirculation gases. The reignition event occurs later allowing the fuel to travel downstream further and more fuel to accumulate. This is possible because the returning wave is not able to ignite the fuel near the backstep at the midpoint of the cycle. After ignition because of the large amount of fuel available, the pressure rise is larger than that observed in the 5.5 in.

A possible explanation of why the 7.5 in configuration is stable experimentally would be the heat loss from the walls. The adiabatic walls used in the simulation predict a higher temperature in the recirculation region. If the reignition mechanism were not present, the large pressure fluctuations that give rise to the starvation event would not occur. Other possibilities include the use of a single step global reaction, it is possible that a chemical kinetics set which can accurately predict the auto-ignition time may be required. A final possibility is the initial condition used (filling the chamber with hot (1500 K) gases). This initial condition may create non-realistic initial transients, which allow a limit cycle to be reached that is self-sustaining. Very likely, a combination of these three issues is the culprit; plans to continue to investigate these in the future are underway.

Acknowledgments

Computing resources were provided by the DoD High Performance Computing Modernization Program.

References

[1]Harrje, D. and Reardon, F., "Liquid Propellant Rocket Combustion Instability," Technical Report SP-194, NASA, Washington D.C., 1972.

[2]Culick, F., "Combustion Instabilities: Mating Dance of Chemical, Combustion, and Combustor Dynamics," *36th Annual AIAA/ASME/SAE/ASEE Joint Propulsion Conference and Exhibit*, Huntsville Alabama, July 2000.

[3]Ducruix, S., Schuller, T., Durox, D., and Candel, S., "Combustion Dynamics and Instabilities: Elementary Coupling and Driving Mechanisms," *Journal of Propulsion and Power*, Vol. 19, No. 5, 2003, pp. 722–734.

[4]Culick, F., "Combustion Instabilities in Liquid-Fueled Propulsion Systems an Overview," Tech. Rep. CP-450, AGARD, 1989.

[5]Culick, F. and Yang, V., *Overview of Combustion Instabilities in Liquid-Propellant Rocket Engines*, chap. 1, AIAA, 1995.

[6]Evesque, S. and Polifke, W., "Low-Order Acoustic Modeling For Annular Combustors: Validation and Inclusion of Modal Coupling," *ASME Turbo Expo*, No. GT-2002-30064, Amsterdam, June 2002.

[7]Culick, F., "Some Recent Results for Nonlinear Acoustics in Combustion Chambers," *AIAA Journal*, Vol. 32, No. 1, January 1994, pp. 146–169.

[8]Miller, K., *Experimental Study of Longitudinal Instabilities in a Single Element Rocket Combustor*, Master's thesis, Purdue University, West Lafayette, IN, May 2005.

[9]Miller, K., Sisco, J., Nugent, N., and Anderson, W., "Combustion Instability with a Single-Element Swirl Injector," *Journal of Propulsion and Power*, Vol. 23, No. 5, 2007, pp. 1102–1112.

[10]Sisco, J., *Measurement and Analysis of Unstable Model Rocket Combustor*, Ph.D. thesis, Purdue University, West Lafayette, IN, August 2007.

[11]Smith, R., Xia, G., Anderson, W., and Merkle, C. L., "Computational Simulations of the Effect of Backstep Height on Non-premixed Combustion Instability," *AIAA Journal*, Vol. 48, No. 9, 2010, pp. 1857–1868.

[12]Yu, Y., *Experimental and Analytical Investigations of Longitudinal Combustion Instability in a Continuously Variable Resonance Combustor (CVRC)*, Ph.D. thesis, Purdue University, West Lafayette IN, April 2009.

[13]Yu, Y., Sisco, J., Rosen, S., Madhav, A., and Anderson, W., "Spontaneous Longitudinal Combustion Instability in a Continuously-Variable Resonance Combustor," *Journal of Propulsion and Power*, Vol. 28, No. 5, 2012, pp. 876–887.

[14]Smith, R., *Computational Investigation of High Frequency Acoustics and Instabilities in a Single-Element Rocket Combustor*, Ph.D. thesis, Purdue University, West Lafayette IN, Aug. 2010.

[15]Smith, R., Xia, G., Anderson, W., and Merkle, C., "Computational studies of the effects of oxidizer injector length on combustion instability," *Combustion Theory and Modeling*, Vol. 12, 2012, pp. 341–368.

[16]Harvazinski, M., *Modeling Self-Excited Combustion Instabilities Using a Combination of Two- and Three-Dimensional Simulations*, Dissertation, Purdue University, West Lafayette, May 2012.

[17]Harvazinski, M., Anderson, W., and Merkle, C., "Analysis of Self-Excited Combustion Instability using Two- and Three-Dimensional Simulations," *Journal of Propulsion and Power*, Vol. 29, No. 2, 2013, pp. 396–409.

[18]Feldman, T., *Unstable Combustion Processes for a Single Element Shear/Coax Injector in a Longitudinal Combustor*, Masters thesis, Purdue University, West Lafayette, May 2013.

[19]Feldman, T., Harvazinski, M., Merkle, C., and Anderson, W., "Comparison Between Simulation and Measurement of Self-Excited Combustion Instability," *48th AIAA/ASME/SAE/ASEE Joint Propulsion Conference and Exhibit*, AIAA, Atlanta, GA, July 2012.

[20]Garby, R., Selle, L., and Poinsot, T., "Analysis of the impact of heat losses on an unstable model rocket-engine combustor using large-eddy simulation," AIAA, Atlanta, GA, July 2012, AIAA Paper 2012-4085.

[21]Garby, R., Selle, L., and Poinsot, T., "Large-Eddy Simulation of Combustion Instabilities in a Variable-length Combustor," *Comptes Rendus Mécanique*, Vol. 341, No. 1-2, 2013, pp. 220–229.

[22]Guézennec, N. and Mennon, S., "Large-Eddy Simulation of Combustion Instability in a High-Pressure Shear-Coaxial Injection Combustor," *Submitted to Combustion and Flame*, 2013.

[23]Li, D., Merkle, C., and Xia, G., "Analysis of Real Fluid Flows in Converging Diverging Nozzles," *33rd AIAA Fluid Dynamics Conference and Exhibit*, June 2003, AIAA Paper 2003-4132.

[24]Li, D., Sankaran, V., Merkle, C., and Lindau, J., "A Unified Computational Formulation for Multi-Component and Multi-Phase Flows," *43rd AIAA Aerospace Sciences Meeting and Exhibit*, January 2005, AIAA Paper 2005-1391.

[25]Lian, C., Xia, G., and Merkle, C., "Solution-Limited Time Stepping to Enhance Reliability in CFD Applications," *Journal of Computational Physics*, Vol. 228, 2009, pp. 4836–4857.

[26]Li, D., Xia, G., Sankaran, V., and Merkle, C., "Computational Framework for Complex Fluids Applications," *3rd International Conference on Computational Fluid Dynamics*, Toronto, Canada, July 2004.

[27]Xia, G., Sankaran, V., Li, D., and Merkle, C., "Modeling of Turbulent Mixing Layer Dynamics in Ultra-High Pressure Flows," *36th AIAA Fluid Dynamics Conference and Exhibit*, San Francisco, CA, June 2006, AIAA Paper 2006-3729.

[28]Lian, C., Xia, G., and Merkle, C., "Impact of Source Terms on Reliability of CFD Algorithms," *The 19th AIAA Computational Fluid Dynamics*, San Antonio, TX, June 2009.

[29]Spalart, P., Jou, W., Strelets, M., and Allmaras, S., "Comments on the feasibility of LES for wings on a hybrid RANS-LES approach," *1st U.S. Air Force Office of Scientific Research Office Conference on DNS/LES*, Columbus, OH, August 1997, pp. 137–148.

[30]Travin, A., Shur, M., and Splart, P., "Physical and numerical upgrades in the detached-eddy simulation of complex turbulent flows," *412 EUROMECH Colloquium on LES of Complex Transitional and Turbulence Flows*, Munich, October 2000.

[31]Wilcox, D., *Turbulence Modeling for CFD*, DCW Industries, 1998.

[32]Wilcox, D., "Formulation of the k-ω turbulence model revisited," *45th AIAA Aerospace Sciences Meeting and Exhibit*, AIAA, Reno, NV, January 2007.

[33]Westbrook, C. and Dryer, F., "Simplified Reaction Mechanisms for the Oxidation of Hydrocarbon Fuels in Flames," *Combustion Science and Technology*, Vol. 27, 1981, pp. 31–43.

[34]Pozrikidis, C., *Fluid Dynamics: Theory, Computation, and Numerical Simulation*, chap. Equations of motion and vorticity transport, Springer, 2nd ed., 2009, pp. 343–350.

[35]Peters, N., "Four Lectures in Turbulent Combustion," *ERCOFTAC Summer School, Aachen Germany*, 1997.

[36]Kuo, K., *Principles of Combustion*, Wiley, 2nd ed., 2005.

[37]Rayleigh, J., "The Explanation of Certain Acoustical Phenomena," *Nature*, Vol. 18, 1878, pp. 319–321.

[38]Nicoud, F. and Poinsot, T., "Thermoacoustic instabilities: Should the Rayleigh criterion be extended to include entropy changes?" *Combustion and Flame*, Vol. 142, 2005.